Cations Stiffen Actin Filaments by Adhering a Key Structural Element to Adjacent Subunits

Glen M. Hocky,[†,#] Joseph L. Baker,[‡,#] Michael J. Bradley,[§,∥] Anton V. Sinitskiy,[†,⊥] Enrique M. De La Cruz,*[,§] and Gregory A. Voth*[,†]

[†]Department of Chemistry, James Franck Institute, Institute for Biophysical Dynamics, and Computation Institute, The University of Chicago, Chicago, Illinois 60637, United States

[‡]Department of Chemistry, The College of New Jersey, Ewing Township, New Jersey 08628, United States

[§]Molecular Biophysics and Biochemistry, Yale University, New Haven, Connecticut 06520, United States

S *Supporting Information*

ABSTRACT: Ions regulate the assembly and mechanical properties of actin filaments. Recent work using structural bioinformatics and site-specific mutagenesis favors the existence of two discrete and specific divalent cation binding sites on actin filaments, positioned in the long axis between actin subunits. Cation binding at one site drives polymerization, while the other modulates filament stiffness and plays a role in filament severing by the regulatory protein, cofilin. Existing structural methods have not been able to resolve filament-associated cations, and so in this work we turn to molecular dynamics simulations to suggest a candidate binding pocket geometry for each site and to elucidate the mechanism by which occupancy of the "stiffness site" affects filament mechanical properties. Incorporating a magnesium ion in the "polymerization site" does not seem to require any large-scale change to an actin subunit's conformation. Binding of a magnesium ion in the "stiffness site" adheres the actin DNase-binding loop (D-loop) to its long-axis neighbor, which increases the filament torsional stiffness and bending persistence length. Our analysis shows that bound D-loops occupy a smaller region of accessible conformational space. Cation occupancy buries key conserved residues of the D-loop, restricting accessibility to regulatory proteins and enzymes that target these amino acids.
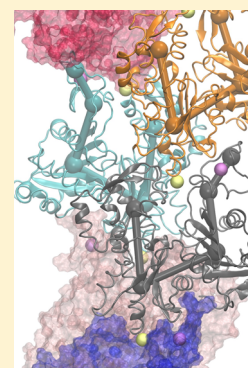
INTRODUCTION

Solution salts are key players in the regulation of the actin cytoskeleton.[1−8] A high affinity (in the nanomolar range) cation is associated with and stabilizes the conformation of a bound nucleotide, which affects actin monomer structure and filament structure and assembly.[2,3,9,10] Low affinity (in the millimolar range) cation interactions induce polymerization and regulate mechanical properties of filaments.[2,4,10] Structural bioinformatics and site-specific mutagenesis experiments favor a mechanism in which occupancy of two discrete low affinity cation binding sites positioned longitudinally between actin subunits drives actin assembly and modulates filament stiffness.[11] These sites have been termed the "polymerization" and "stiffness" sites based on the effect of amino acid substitutions on *in vitro* assembly and filament rigidity.[11] Structural approaches to date, including X-ray crystallography and cryo-electron microscopy, have been unable to resolve filament-associated cations, which has limited understanding of the molecular origins underlying these two observed behaviors.[12]

Computer simulations have proven to be a powerful tool to understand the molecular determinants of actin structural dynamics and allostery, as well as how these are influenced by interactions with regulatory proteins and small molecule cofactors (e.g., adenine nucleotides, ATP and ADP, or ADP together with the phosphate anion formed by ATP hydrolysis).

For example, these simulations have verified the dependence of actin monomer conformations on bound nucleotide identity, initially identified by X-ray crystallography,[13] and delineated the mechanism of bound ATP chemical cleavage, thereby explaining the large difference between monomer and filament nucleotide hydrolysis rates.[14] Furthermore, simulations reliably capture nucleotide- and regulatory protein-dependent actin filament bending and torsional stiffness, with absolute persistence length values that agree remarkably well (within a factor of 2) with "wet-lab" determinations, despite the experiment and simulation sampling greatly different time scales.[15] Filaments with bound ADP are more compliant in bending and twisting than those with bound ATP; filaments with bound cofilin are even more flexible.[16−20] Molecular dynamics (MD) simulations predict that this behavior arises from differential folding of the actin DNase-binding loop (D-loop),[21] consistent with electron microscopy studies implicating this subdomain in regulating filament structure and mechanics.[22]

Despite the evidence showing that discrete cation binding plays a critical role in regulating filament polymerization and mechanics, no computational study to date has included

coordinating divalent cations in the stiffness and polymerization sites predicted by biochemical experiments. A computational study can allow for a detailed molecular understanding of the binding modalities and residues involved, which can inform and drive future experimental studies. In this work, we construct simulation models including coordinated magnesium ions between actin subunits. We have three goals: [1] evaluate whether structural models of cation binding sites on filaments are plausible, [2] examine in molecular detail the structural changes that must occur at the interface between actin subunits to accommodate coordinated cations, and [3] determine the effects of cation occupancy on filament mechanical properties. We show that proposed cation sites are indeed reasonable, and that they stiffen actin filaments by adhering the actin D-loop to the adjacent actin's target binding cleft (TBC).

■ METHODS

System Construction and Simulation Details. Atomistic models of actin filaments are prepared as in previous studies[23,24] and as described in the Supporting Information (SI). In brief, the configuration of an actin subunit is formed into a filament structure by repeated translation and rotation. In the case of a pure actin filament, this consists of a shift of 27.6 Å and a rotation of 166.6° such that the actin double helix makes one right-handed half-turn every 13 subunits. In this paper, we create and study six different actin filament conformations by molecular dynamics simulations. Two of the systems are built from the Namba filament model.[25] The first is constructed as described in refs.[23,24] (termed Namba, throughout). For the second, and the main object of our study, a new model subunit must be engineered to accommodate two additional cations per subunit, with bridging longitudinal intersubunit interactions (termed Namba-cation. See Figure 1 and discussion in the Results section). The third and fourth systems are filaments constructed for reference from the Oda model.[26] The former is built as in previous studies[23,24] (Oda), and the second contains a bound stiffness magnesium ion designed to mimic the coordination produced in the Namba filament, as described in the Results section (Oda-cation). Additionally, we reanalyze D-loop conformations from previous simulations of an Oda filament engineered to contain a folded D-loop from the 1J6Z structure[27] as in ref 21 (Oda-f), and the simulations in ref 16 of a cofilin-bound actin filament with 11 subunits (Cofilin). All actin subunits in this study contain a bound ADP and coordinating Mg^{2+} ion in the nucleotide-binding cleft.

Simulations were performed as in previous studies (e.g., ref 24) using the CHARMM27+CMAP force field[28] with explicit TIP3P water molecules[29] using NAMD.[30] The system was ionized with monovalent ions to a concentration of 0.180 M KCl using VMD.[31] Simulations employed electrostatics treated with Particle Mesh Ewald method[32] with a 12 Å cutoff. Simulations were performed at 310 K and 1 atm with temperature maintained using a Langevin thermostat[30] with a coefficient of 5 ps^{-1} and pressure maintained by a Langevin piston[33] with a period of 2 ps and a time constant of 1 ps.

Specialized Analysis. *Coarse-Grained Actin Mapping.* To facilitate analysis of our atomistic data, we map our simulation data to a coarse-grained representation using the 12-site mapping defined in Saunders and Voth (Table S3).[24] In this mapping, the traditional definitions for the four subdomains (SD) of actin are preserved, while several important components such as the SD2 D-loop, are broken out into separate beads such that their fluctuations can be resolved. The
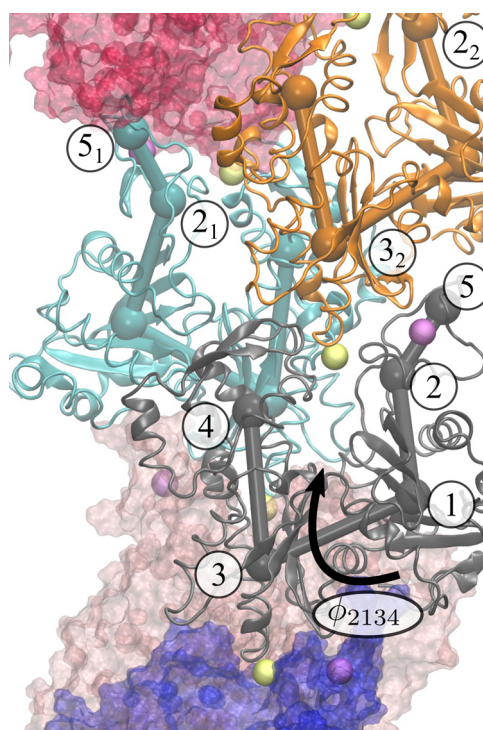

Figure 1. Polymerization (yellow) and stiffness (purple) cations are added in putative binding sites between actin subunits in the positions shown. Beads labeled 1−4 show the center of mass positions of the four actin subdomains as defined in Table S3, while bead 5 shows the center of mass of the D-loop (residues 40−51). A subscript indicates the relative subunit position in the filament (increasing toward the "pointed" end). Also shown is the φ_{2134} dihedral angle, which is used to measure the planarity of an actin monomer.

position of each coarse-grained bead is defined as the center of mass of the residues specified in Table S3. For nomenclature, when computing intersubunit quantities, we refer to a bead on one actin simply by its number, and to a position on the second actin by its number and a subscript indicating its relative subunit index, increasing toward the pointed end of the filament (see Figure 1).

Magnesium Binding Geometry. To quantify the amount of symmetry found in the coordinating oxygen atoms around the Mg^{2+} ions, we compute the Q_4 variant of the Steinhardt-Nelson bond-orientational order parameter.[34] Using this formula, we calculate that a perfect octahedral geometry formed by six coordinating oxygen atoms will have a Q_4 value of 0.764, and distorted structures will have smaller values. Coordination with no 4-fold symmetry would have a Q_4 value near zero. See SI for further details.

Dimensionality Reduction Techniques. To identify the effects of specific cation binding on the conformations of the D-loop without imposing any presupposed interpretations, we use statistical techniques to automatically classify the D-loop states observed in simulation. We employ two different methods to help to ensure our conclusions are independent of our method of analysis. The first technique is Dihedral Principal Component Analysis (dPCA).[35] In this method, we perform standard principal component analysis on cosines and sines of the φ, ψ, and ω backbone dihedral angles internal to the 12 residues in the D-loop. Singular value decomposition is performed on this matrix to extract linear combinations of the cosines and sines of the dihedral angles that contain the
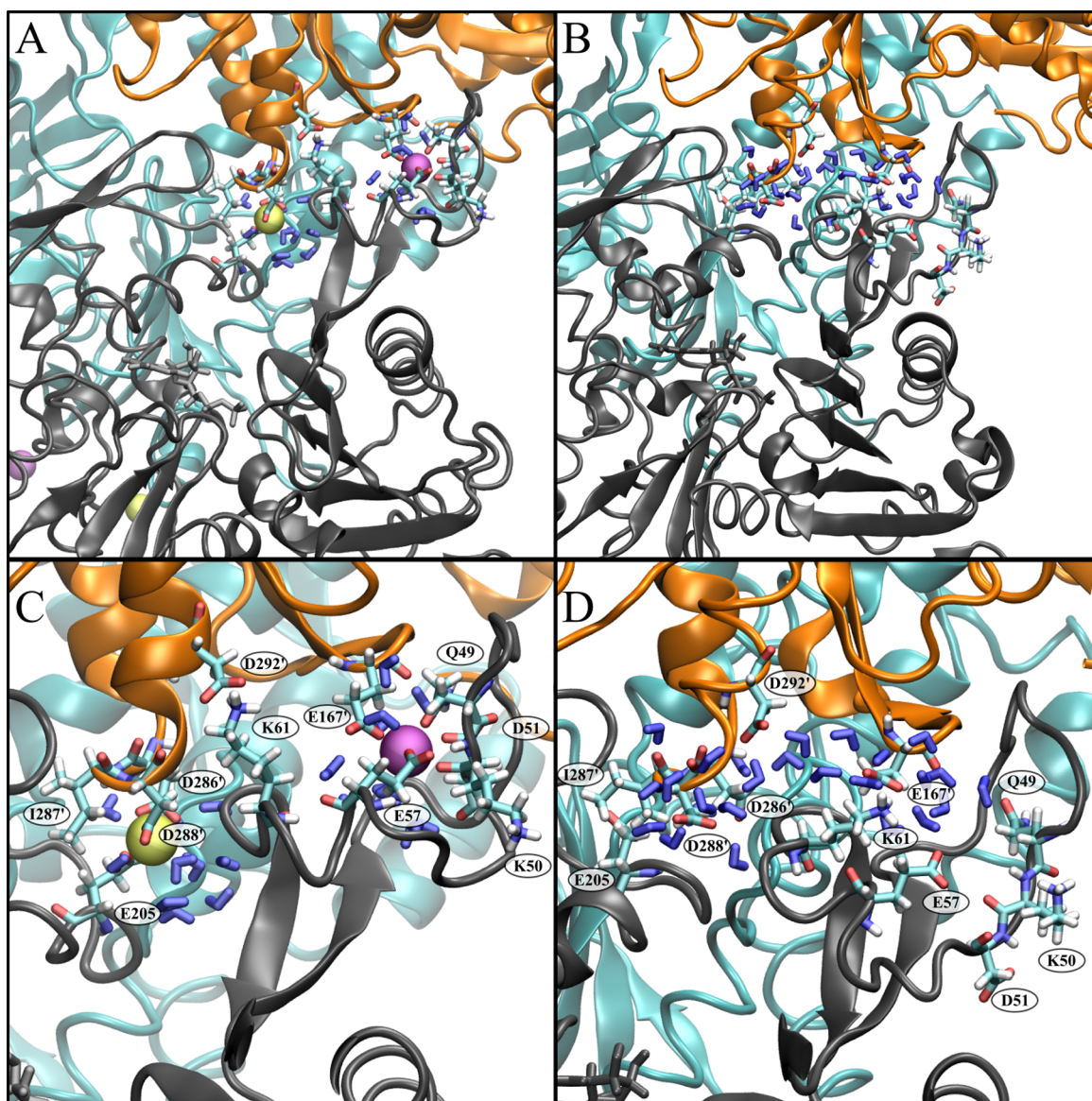
Figure 2. Typical snapshots from simulations of the Namba model with (A,C) and without (B,D) additional coordinated Mg^{2+} ions. Panels A and B show an overview, and C and D show a closer view. (A,C) Polymerization cations shown in yellow, and stiffness cations are shown in purple. Protein residues and water molecules within 5 Å of the central cations are atomically resolved, as are residues D292′ and K61, which form a salt bridge when the stiffness ion is added. (B,D) Residue positions that will form the core of the polymerization site (E205, D286′, D286′, and I287′) and form the stiffness site (Q49, K50, D51, E57, E167′) are shown in detail, as well as water within 5 Å of D286′, D288′ and E167′. The side chain of K61 is oriented such that it forms a salt bridge with E167′.

most information about the variance found in the data set. The values of the top few principal components can often be used to identify clusters in a set of data, which in a molecular context can help identify discrete conformational states of a protein of interest.[35] The second technique employed is the Diffusion Map (DM) approach.[36,37] Here, we compute the pairwise RMSDs of all D-loop configurations, superposing each configuration using the Theobald QCP Algorithm[38] as implemented in the MDTraj library.[39] A matrix of squared distances is constructed, exponentiated, and diagonalized. The eigenvectors with the largest eigenvalues can be used, in a manner similar to principal components, to separate structures that have distinct conformations. Details for both analyses can be found in the SI.

Computing Filament Properties. The persistence length of filaments is computed by fitting the decay of bending fluctuations along the filament to an exponential function.[23] In order to do this, the center-of-mass (COM) of the subunit positions in the two (A and B) strands of the actin helix are mapped to a central "strand" running up the center of the filament. This procedure is performed as in ref 23 on a series of 10 ns windows, and the average and standard deviation among different time windows is computed. To extract the torsional rigidity, we compute the variance of twist angles in the filaments as in ref 40, where here the twist angle is defined (with the long axis of the filament aligned along the z-axis) as the angle α between adjacent interstrand vectors pointing from the COM of one actin monomer to another (e.g., r_{12} and r_{34}) projected in the xy plane. We can then compute the torsional rigidity as $C = k_B T d/\sigma^2$, where d is the average distance between the COM of subunits in the same strand, and σ is the standard

deviation in the twist angles, α, in a single filament snapshot obtained from the simulations.

■ RESULTS AND DISCUSSION

Construction of "Stiffness" and "Polymerization" Cation Binding Sites. In order to generate cation binding geometries for the stiffness and polymerization sites, we first had to insert magnesium ions into a structural model for an actin filament near candidate binding pocket sites. Several actin filament models exist, e.g., refs 25, 26, 41, and 42, and all of these share many general features while having some small differences (e.g., older models contained a structured N-terminus in each subunit, and the Namba model favors longitudinal contacts over lateral contacts by a small subunit; see refs 24 and 42). In this work, we chose to initially construct our cation binding sites from the Namba filament model[25] for two reasons. First, as the filaments used to generate the original Namba model were selected to make "F-actin as straight as possible", we suspect that geometry represents a more rigid subpopulation of actin geometries as has been suggested before.[25,43] Hence, the Namba model may be more representative of actin filament structures found under high divalent-cation conditions. Second, the stiffness site amino acid side chains and backbone atoms in the Namba model are nearly positioned in an ideal binding geometry for a magnesium ion and, hence, require minimal perturbation to make these cation insertions. In particular, Glu167′ (the single tick referring to a position a subunits two away in the pointed-end direction), is strongly indicated as being involved in this interaction, is far more proximal to the center of the predicted binding pocket in the current Namba geometry (Table S1).

Mg^{2+} binding geometries of structures in the PDB[44] generally contain six coordinating oxygen atoms in an octahedral geometry, with two of the oxygen atoms coming from contacts with water molecules. To construct a Namba filament with bound stiffness and polymerization ions, pentamers of the Namba model were built with Mg^{2+} ions inserted in the three actin−actin longitudinal interfaces, near to the residues implicated in ion binding.[11] We then performed a series of minimization and molecular dynamics simulations with additional harmonic biases added to the simulation force field, which moved oxygen atoms from selected side chains to be consistent with hexa-coordination (see SI and Table S2), with water molecules to be inserted later in the remaining two spots. Further restraints were applied to bring the D-loop (residues 40−51) in further contact with residues in the proximal actin Subdomain 3, which proved necessary to prevent the D-loop from collapsing in a manner not observed in known structures of actin. The particular choice of residues to include in stiffness and polymerization ion coordination was based first on experimental constraints and bioinformatics data in refs 2 and 11 with a preference for residues having high sequence conservation among actin structures.[2] The distances to be restrained were iterated many times until reaching a geometry ensuring the Mg^{2+} cations remain in the binding pocket over many nanoseconds. We note that the resulting D-loop configuration is similar to that observed in a recent structure of actin complexed with tropomyosin.[45] Finally, we constructed a periodic 13-subunit filament based on the configuration of the central actin subunit, and confirmed that Mg^{2+} remain bound in the two actin binding pockets for hundreds of nanoseconds. This 13-subunit filament was used for all subsequent analysis.

To further confirm the effect of stiffness ion occupancy on filament rigidity, we built a 13-subunit Oda filament with bound stiffness ion employing the same distance constraints and minimization protocol as one used to build the Namba-cation model. The resulting starting configuration also held stiffness ions in place for >150 ns. However, the side chain geometry around the magnesium ion in the Oda-cation model is not as stable as in the Namba-cation model. Moreover, the construction protocol destabilized other contacts in the Oda system, such that drifts in coarse-grained observables, could be observed over long simulations. Hence, since this structure would require additional manipulation to produce a fully stable initial geometry, we do not examine this simulation in detail any further, but only include calculations of persistence length and torsional rigidity for the early period of the simulation where coordination and filament properties appear stable.

The details of the minimization protocols employed here, including considerations when choosing the distances to constrain, and the force constants used to enforce the constraints, are detailed in the SI. Additionally, the SI contains a PDB file of an equilibrated 13-subunit filament Namba-cation and Oda-cation filaments with ions produced by these procedures.

Magnesium Binding Sites. The constructed "polymerization" and "stiffness" cation binding sites of our Namba-cation model relax in the first few nanoseconds of simulation. Typical snapshots of the ion binding sites from the Namba and Nation-cation systems are compared in Figure 2, and are discussed in detail below. Considering oxygen−magnesium distances within 3 Å as interactions, both magnesium ions remain stably bound in an octahedral geometry with six coordinating oxygen atoms for more than 200 ns of subsequent dynamics. The binding geometry in the Stiffness (S) site stays more symmetric and more similar to ideal octahedral binding than does the Polymerization (P) site (Figure 3A), as assessed by measuring the Steinhardt-Nelson order parameter, Q_4 (see Methods section and the SI for further details).[34] Most of the amino acid residues hypothesized to be involved in cation coordination proved reasonable (Figure 2). However, some significant differences did emerge from the simulations, as discussed below.

Stiffness Site. We compute cation coordination in the Namba-cation system every 50 ps after waiting 75 ns for the binding pockets to find their preferred conformations. The stiffness site cation maintained its full initial coordination with residues Q49, K50, E57, and E167′ and two water molecules for 70% of the simulation time. Among these snapshots of the stiffness ion coordination, 15% have K50 replaced by an interaction with the neutral side chain oxygen of E167′. In one of the 13 stiffness sites in the periodic filament, the Q49 side chain was replaced by a water oxygen in the first 50 ns; subsequently, the K50 interaction was lost in the next 25 ns and replaced by a water molecule. Hence, for the final 150 ns of simulation, 1/13 of the magnesium sites is coordinated only by E57 and E167′. In no case was a simulation snapshot observed lacking a bound E167′ oxygen, consistent with this residue playing a critical role in cation coordination.[11]

Polymerization Site. Every polymerization site magnesium ion was initially coordinated by four side chain oxygen atoms and two water oxygen atoms in the equilibrated Namba-cation filament model. For simulation times following the 75 ns of binding equilibration, ∼ 72% of the magnesium ions are bound by five side chain oxygen atoms and one water oxygen. Sixty-
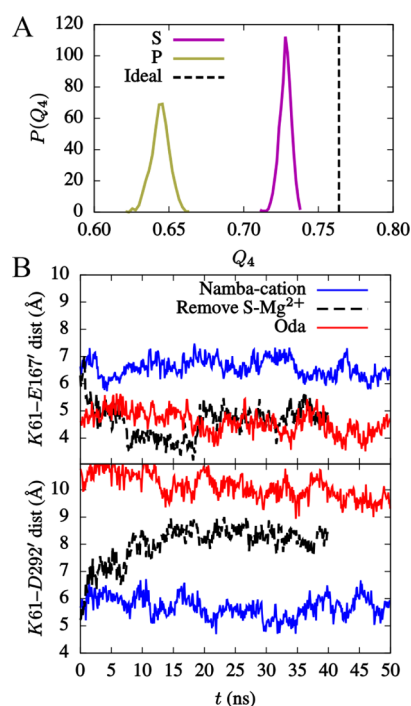
Figure 3. (A) Cation binding geometry is six coordinate and has high symmetry. Vertical dashed line shows the value of Q_4 for an ideal octahedron. The polymerization site (P), while still symmetric, is more distorted than the binding in the stiffness site (S). (B) Distance between charged atoms in residues suspected to form a salt bridge in actin. Top—salt bridge forms after removal of stiffness site Mg^{2+} ion. Bottom—alternative salt bridge is persistent in the cation-coordinated system, and breaks when the stiffness ions are removed.

five percent of the configurations are found with double coordination (associated with both the charged and uncharged side chain oxygen) by D286′ and E205′ with a single coordinating D288′, while, in the remaining cases, the magnesium is doubly bound by D288′ and singly bound to D286′. The remaining 28% of coordination sites cases are split ~18% with two bonds to E205 and one each to D286′ and D288′, and ~10% doubly bound to D286′, and singly bound to D288′ and E205′.

Although it was biased to be included in the initial binding, T202 did not directly coordinate the polymerization site ion. In the Namba filament without magnesium ions, the side chain of T202 formed H-bonds with D286′ occasionally, and virtually never with any other binding partner, while in our Namba-cation model hydrogen bonding was observed with subunit i+2 residue D286′ and also with side chains of subunits i+1 residues S271 (as previously observed, e.g., in ref 42) and D179 and the backbone of E270 (as seen, e.g., in ref 26). Phosphorylation of T202 affects filament elongation.[46,47] Our Namba-cation model simulations suggest that these effects could potentially arise by indirectly compromising magnesium coordination at the polymerization site.

On the K61-E167′ Salt Bridge. Kang et al.[12] have noted that the existence of the E167′-magnesium interaction precludes the K61-E167′ salt bridge present in other actin filament models,[25,42,45] including our Namba and Oda filaments lacking coordinated Mg^{2+} in the stiffness sites (Figure 2B). To ensure that we have not excluded this important salt-bridge interaction through our choice of molecular mechanics force field, we performed one simulation where we removed the 13 stiffness

site Mg^{2+} ions after simulation for 200 ns (26 random Cl^- ions more than 10 Å from the filament were also removed to maintain neutrality; this does not substantially change the monovalent salt concentration). The distance between the K61 and E167′ side is stable in the magnesium-bound simulation, but relaxes in just a few nanoseconds to the salt-bridge distance observed in the Oda model after the magnesium ions are removed (Figure 3B). In the cation-bound system, an alternative salt bridge between K61 and D292′ is formed (Figure 2A).

Filament Conformational Changes. To determine the extent to which our addition of coordinated magnesium ions influences the actin subunit and filament conformation, it is most insightful to look at distributions of coarse-grained observables. Two of the most relevant ones are the distribution of the twist angle (the rotation between adjacent subunits) and the subunit separation in the longitudinal direction ("rise") observed in the filament. We observe that adding coordinated Mg^{2+} ions to the Namba filament narrows the distribution of actin twist angles (Figure 4A). It also results in a slightly more broad distribution of rise distances, with more density in small intersubunit distance range (Figure 4B). This is likely a simple consequence of stronger longitudinal interaction strength. Another major consideration is whether adding these coordinated ions modifies the individual subunit flatness, which can be measured by the φ_{2134} dihedral angle between the four coarse-grained sites representing actin subdomains 1–4 (see Figure 1). There is little difference in our two Namba filament models (Figure 4C), indicating that the addition of these ions does not have a large effect on subunit conformation, especially when compared to the more substantial perturbation of binding cofilin (short dashed line).

To ascertain the effect of the polymerization ion on subunit conformation, we have examined all of the distributions of coarse-grained distances and angles containing coarse-grained domains 2, 4, and 3_2, between which it is situated (see Figure 1). We find little difference in the quantities, in particular the direct distance between domains 2 and 4 (not shown), and the angle formed between these three domains hardly changes on inclusion of the polymerization site ion (Figure 4D), and conclude that this addition largely imposes a local backbone rearrangement to accommodate a different packing of side chains.

The stiffness cation has a very large effect on the longitudinal interaction between subunits. It substantially reduces the distance between the D-loop and SD3 (Figure 4E), and results in a much tighter distribution, indicating a much stronger interaction between these two components. The decreased flexibility of the D-loop can also be corroborated by looking at the distribution of intra-actin distances between the D-loop and the center of mass of SD2, which is also substantially reduced in width (Figure 4F).

D-Loop Conformational Changes. To accommodate the additional coordination of the stiffness cation between the actin D-loop and SD3, the D-loop loses great deal of its flexibility and is much more strongly coordinated to the i+2 target binding cleft as discussed in the previous section. To quantify this effect, we used VMD[31] to compute the solvent-accessible surface area (SASA) of the D-loop in actin i that is buried by actin i+2 by computing the difference in SASA between the D-loop alone and the SASA of the D-loop in the presence of the rest of the actin (Table 1 and Table 2). We find that our Mg^{2+}-bound Namba filaments have substantially less accessible
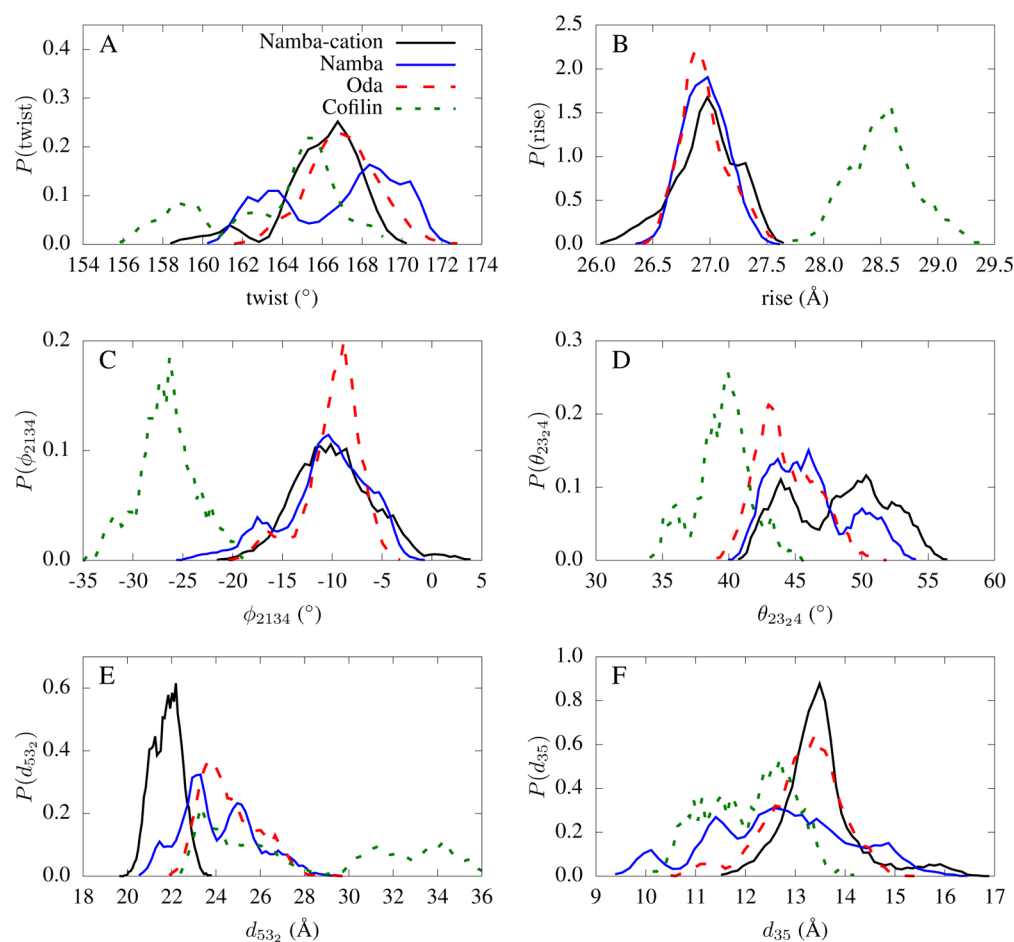
Figure 4. Coarse-grained distribution functions. Coarse-grained subunit definitions are illustrated in Figure 1. (A) Twist angle between adjacent subunits in the filament. (B) Average longitudinal distance between adjacent actin subunits in the filament. (C) Flattening dihedral angle in the actin subunits. (D) Angle formed between subdomains 2 and 4 in an actin filament, and subdomain 3 in the actin two subunits away. (E) Distance between the actin D-loop and the coordinated subdomain 3. (F) Distance within a subunit between subdomain 3 and the center-of-mass of the D-loop.

Table 1. D-Loop Surface Area Buried by SD3 in Adjacent Actin

system	buried surface area (Å^2)
Namba-cation	604 ± 63
Namba	418.4 ± 120
Oda	330 ± 176
Cofilin[a]	101 ± 99

[a]In the cofilin bound cases, some of the surface area is instead in contact with cofilin; it is not totally solvent exposed.

Table 2. D-Loop Surface Area of Specific Residues in the D-Loop Buried by SD3 in Adjacent Actin

Residue	Namba-cation	Namba	Oda	Cofilin[a]
Val 43	66 ± 28	61.6 ± 37	67.8 ± 42.5	3 ± 9
Met 44	166 ± 25	77.3 ± 60	47.5 ± 49.6	9 ± 19
Val 45	115.6 ± 37	108.5 ± 32	95.1 ± 51.6	14 ± 23
Met 47	129.3 ± 29	72.6 ± 57	50.1 ± 45.5	51 ± 50

[a]In the cofilin bound cases, some of the surface area is instead in contact with cofilin; it is not totally solvent exposed.

surface area compared to our Namba system without Mg^{2+}. Moreover, access is restricted to important conserved residues in the D-loop, which presumably accounts for inhibition of

cofilin binding[48] and may regulate interaction with other regulatory proteins. For example, Met44 (and Met47) oxidation by Mical can promote filament disassembly.[49] Our results suggest strongly that the susceptibility of these residues to Mical oxidation would be strongly reduced under high divalent cation concentrations (see also ref 45).

To investigate how Mg^{2+} modulates the conformations accessed by the D-loop, we study the conformations using dPCA and DM (Figure 5). We include additional simulations of filaments with folded D-loops to expand the types of structures that can be identified. The dPCA analysis shows that the D-loop can adopt several distinct conformational in filaments. The D-loop conformations explored in our Namba-Mg^{2+} simulations are predominately similar to unfolded D-loop conformations observed in the standard Namba and Oda simulations. Our dPCA and DM data do show that our standard Namba simulations explore some cofilin-like and folded-like structures (although none are classified as having helical content by the STRIDE algorithm[50]).

The DM indicates that the addition of Mg^{2+} ions restricts the conformations accessed to one "corner" of available state space. Hence, Mg^{2+} occupancy restricts the entropy of the D-loop conformational ensemble, as compared to the standard Namba filament. The thermodynamically linked dissociation of magnesium ions[12] and subsequent D-loop disorder presumably
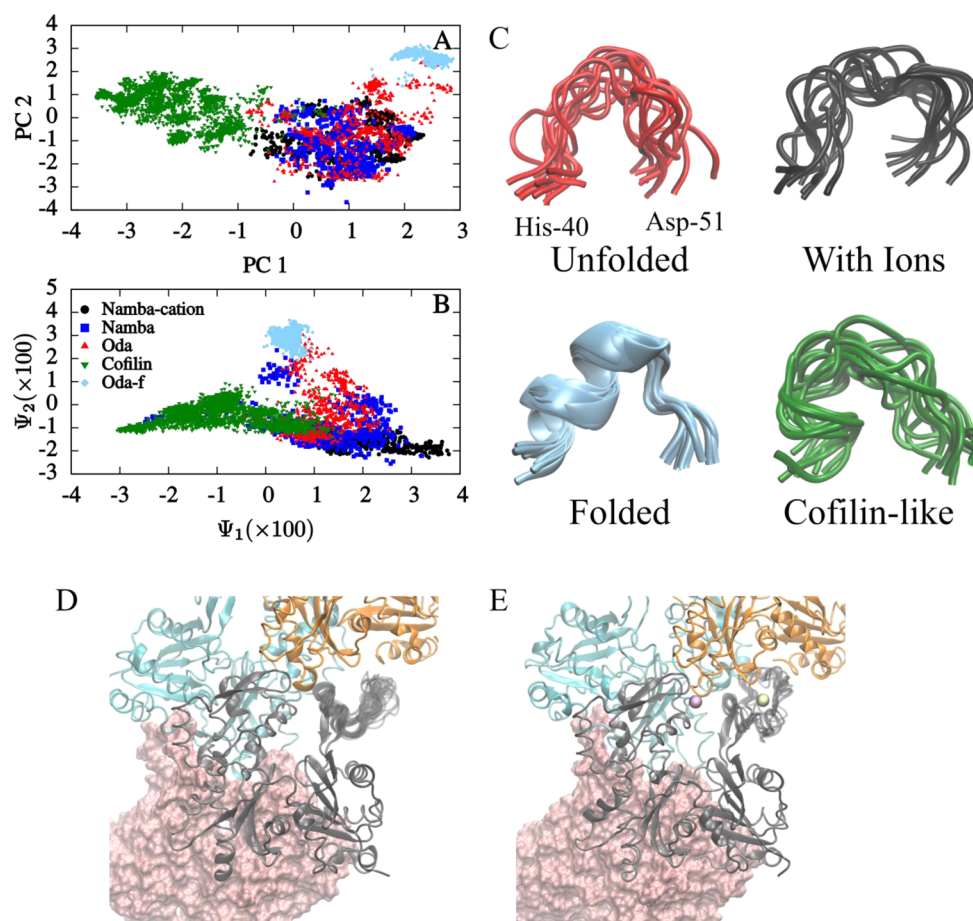
Figure 5. D-loop fluctuations. (A) First two principal components from dPCA analysis reveal three states, folded, unfolded and cofilin-like. (B) DM analysis confirms existence of same three states. Results for filament with coordinated Mg^{2+} are restricted to a subset of unfolded structures. (C) Typical snapshots taken from the different states identified in (A). All are oriented from N-term to C-term going from left to right. Unfolded conformations have PC1 > −1 and PC2 < 2, folded conformations have PC > 2.5, and cofilin-like structures have PC1 < −1. (D,E) Interface between segments with and without coordinated stiffness ion. Twenty snapshots for D-loop and adjacent residues (40−62) are shown every 2.5 ps from a representative molecular dynamics trajectory. The D-loop conformations in the ion-bound system are more tightly bound to the adjacent subdomain 3 (Figure 4).

contribute to the positive entropy associated with cofilin binding.[12]

Filament Rigidity. Cations increase the filament bending persistence length and torsional rigidity relative to the Namba filaments from which they have been constructed (Table 3). The Namba-cation model shows a persistence length increase

Table 3. Mesoscopic Mechanical Properties of Actin Filaments[a]

	L_p (μm)	rigidity (10^{-26} Nm^2/rad)
Namba-cation	12.6 ± 2.8	0.54 ± 0.10
Namba	7.98 ± 0.88	0.43 ± 0.07
Oda-cation	8.13 ± 1.66	0.51 ± 0.16
Oda	5.60 ± 0.78	0.25 ± 0.04
measured, high salt	10.5 ± 1.5[11]	–
measured, low salt	3.6 ± 0.5[11]	0.23 ± 0.1[51,52]

[a]Persistence length and torsional rigidity were computed on 10 ns sliding windows (with a 5 ns shift) covering simulation times from 10 to 60 ns. The values reported are the average and standard deviation from the different time windows. Measured values from Kang et al.[11] represent the lowest persistence length observed and an extrapolation to saturating divalent cation conditions in that work.

comparable to that observed in "wet-lab" experiments varying divalent cation concentration.[11] We note that the values from ref 11 in Table 3 correspond to low monovalent salt concentrations, while our simulations correspond to a physiological monovalent salt concentration where the filament starts out in a more rigid state, and hence we would not expect as large of a fractional increase in persistence length. Our results do suggest that the increase in stiffness from coordinating magnesium ions can occur at higher concentrations of KCl than were studied in that work.

For both the Namba and Oda case, we predict an increase in torsional rigidity in addition to the increase in persistence length. We note that for the data in Table 3 we compute overall filament properties in the first part of our simulation to ensure that the results refer to the precise state of the system that we constructed. The increase in stiffness due to addition of magnesium ions persists for the duration of the simulations run (Table S4).

CONCLUSIONS

In this work, we have built an all-atom structural model of actin filaments consistent with experimental observations that suggest the existence of specific cation binding modalities in

filamentous actin. Using molecular dynamics simulations, we have been able to refine hypotheses on which residues are likely to play an important role in the specific ion binding. The model generated in this manner is stable for hundreds of nanoseconds, although it likely represents only one of some number of states that the actin filament can interconvert between on longer (ms to s) time scales.[53] Our simulations exhibit an increase in torsional rigidity and persistence length of the filament, reaching values similar to what is seen in experiment and certainly reproducing the observed experimental trends.

All magnesium ions in the stiffness site remained bound stably for over 200 ns of simulation, but we did observe a deviation from an ideal octahedral side-chain coordination by four actin oxygen atoms. While this is not altogether unusual, we can also speculate that our Namba filament (as well as the original model[25]) has been constructed with bound ADP, while the stiffness ion is coordinated during initial polymerization of ATP-bound monomers. Having a bound cation in a slightly destabilized binding geometry after ATP hydrolysis could be another mechanism by which actin filaments promote depolymerization.

Our results suggest that only a particular subpopulation of D-loop conformations will be accessed when filaments contain coordinated divalent cations in the predicted stiffness site. The change in the conformational ensemble accessible when ion-coordinated versus when bound by cofilin may partially contribute to the positive entropic contributions associated with cofilin binding.[48] We also see restricted access to conserved D-loop residues, which presumably slows cofilin binding kinetics.[48] We predict that at high divalent cation concentrations the accessibility of the D-loop to enzymes that modify residues on it (e.g., Mical) decreases.

The existence of discrete D-loop states and the fact that each D-loop and polymerization site can exist in a discrete bound or unbound state could be incorporated into coarse-grained models for actin filaments, e.g., through the recently developed ultracoarse-graining methodology.[54,55] Due to the intrinsically spatially heterogeneous way in which ion binding might affect filament stiffness, such behavior is likely to have important and interesting consequences for designing large multiscale, coarse-grained simulations of actin networks.

It seems that cytoskeletal networks have adopted a simple modality by which adjusting ion concentration can change material properties on very long (up to micrometer) length scales, as well as yet another way to modify rates in a complex regulatory network controlling their assembly and disassembly. We also believe this structural motif to be a useful guide for those who might hope to design adaptive materials inspired by biological paradigms.

ASSOCIATED CONTENT

ⓢ Supporting Information

The Supporting Information is available free of charge on the ACS Publications website at DOI: 10.1021/acs.jpcb.6b02741.

> Document containing additional methodological details and supporting data (PDF)
> PDF file for equilibrated Namba-cation structure (ZIP)
> PDF file for equilibrated Oda-cation structure (ZIP)

AUTHOR INFORMATION

Corresponding Authors

*E-mail: enrique.delacruz@yale.edu; phone: (203) 432-5424.

*E-mail: gavoth@uchicago.edu; phone: (773) 702-9092.

Present Addresses

∥Syros Pharmaceuticals, Cambridge, MA

⊥Department of Chemistry, Stanford University

Author Contributions

#These authors contributed equally.

Notes

The authors declare no competing financial interest.

REFERENCES

(1) Pollard, T. D.; Blanchoin, L.; Mullins, R. D. Molecular Mechanisms Controlling Actin Filament Dynamics in Nonmuscle Cells. *Annu. Rev. Biophys. Biomol. Struct.* **2000**, *29*, 545−576.

(2) Kang, H.; Bradley, M. J.; Elam, W. A.; De La Cruz, E. M. Regulation of Actin by Ion-Linked Equilibria. *Biophys. J.* **2013**, *105*, 2621−2628.

(3) Estes, J. E.; Selden, L. A.; Kinosian, H. J.; Gershman, L. C. Tightly-bound Divalent Cation of Actin. *J. Muscle Res. Cell Motil.* **1992**, *13*, 272−284.

(4) Strzelecka-Golaszewska, H.; Prochniewicz, E.; Drabikowski, W. Interaction of Actin with Divalent Cations. I. The Effect of Various Cations on the Physical State of Actin. *Eur. J. Biochem.* **1978**, *88*, 219−227.

(5) Frieden, C. The Mg2+-Induced Conformational Change in Rabbit Skeletal Muscle G-Actin. *J. Biol. Chem.* **1982**, *257*, 2882−2886.

(6) Zimmerle, C. T.; Patane, K.; Frieden, C. Divalent Cation Binding to the High- and Low-Affinity Sites on G-actin. *Biochemistry* **1987**, *26*, 6545−6552.

(7) Orlova, A.; Egelman, E. H. A Conformational Change in the Actin Subunit can Change the Flexibility of the Actin Filament. *J. Mol. Biol.* **1993**, *232*, 334−341.

(8) Strzelecka-Golaszewska, H.; Wozniak, A.; Hult, T.; Lindberg, U. Effects of the Type of Divalent Cation, Ca2+ or Mg2+, Bound at the High-Affinity Site and of the Ionic Composition of the Solution on the Structure of F-actin. *Biochem. J.* **1996**, *316*, 713−721.

(9) Gershman, L. C.; Selden, L. A.; Estes, J. E. High Affinity Binding of Divalent Cation to Actin Monomer is Much Stronger than Previously Reported. *Biochem. Biophys. Res. Commun.* **1986**, *135*, 607−614.

(10) Carlier, M. F. Actin: Protein Structure And Filament Dynamics. *J. Biol. Chem.* **1991**, *266*, 1−4.

(11) Kang, H.; Bradley, M. J.; McCullough, B. R.; Pierre, A.; Grintsevich, E. E.; Reisler, E.; De La Cruz, E. M. Identification of

Cation-Binding Sites on Actin that Drive Polymerization and Modulate Bending Stiffness. *Proc. Natl. Acad. Sci. U. S. A.* **2012**, *109*, 16923−16927.

(12) Kang, H.; Bradley, M. J.; Cao, W.; Zhou, K.; Grintsevich, E. E.; Michelot, A.; Sindelar, C. V.; Hochstrasser, M.; De La Cruz, E. M. Site-Specific Cation Release Drives Actin Filament Severing by Vertebrate Cofilin. *Proc. Natl. Acad. Sci. U. S. A.* **2014**, *111*, 17821−17826.

(13) Pfaendtner, J.; Branduardi, D.; Parrinello, M.; Pollard, T. D.; Voth, G. A. Nucleotide-Dependent Conformational States of Actin. *Proc. Natl. Acad. Sci. U. S. A.* **2009**, *106*, 12723−12728.

(14) McCullagh, M.; Saunders, M. G.; Voth, G. A. Unraveling the Mystery of ATP Hydrolysis in Actin Filaments. *J. Am. Chem. Soc.* **2014**, *136*, 13053−13058.

(15) Chu, J.-W.; Voth, G. A. Allostery of Actin Filaments: Molecular Dynamics Simulations and Coarse-Grained Analysis. *Proc. Natl. Acad. Sci. U. S. A.* **2005**, *102*, 13111−13116.

(16) Fan, J.; Saunders, M. G.; Haddadian, E. J.; Freed, K. F.; De La Cruz, E. M.; Voth, G. A. Molecular Origins of Cofilin-Linked Changes in Actin Filament Mechanics. *J. Mol. Biol.* **2013**, *425*, 1225−1240.

(17) Pfaendtner, J.; De La Cruz, E. M.; Voth, G. A. Actin filament remodeling by actin depolymerization factor/cofilin. *Proc. Natl. Acad. Sci. U. S. A.* **2010**, *107*, 7299−7304.

(18) Graham, J. S.; McCullough, B. R.; Kang, H.; Elam, W. A.; Cao, W.; De La Cruz, E. M. Multi-Platform Compatible Software for Analysis of Polymer Bending Mechanics. *PLoS One* **2014**, *9*, e94766.

(19) McCullough, B. R.; Blanchoin, L.; Martiel, J.-L.; De La Cruz, E. M. Cofilin Increases the Bending Flexibility of Actin Filaments: Implications for Severing and Cell Mechanics. *J. Mol. Biol.* **2008**, *381*, 550−558.

(20) McCullough, B. R.; Grintsevich, E. E.; Chen, C. K.; Kang, H.; Hutchison, A. L.; Henn, A.; Cao, W.; Suarez, C.; Martiel, J.-L.; Blanchoin, L.; et al. Cofilin-Linked Changes in Actin Filament Flexibility Promote Severing. *Biophys. J.* **2011**, *101*, 151−159.

(21) Pfaendtner, J.; Lyman, E.; Pollard, T. D.; Voth, G. A. Structure and Dynamics of the Actin Filament. *J. Mol. Biol.* **2010**, *396*, 252−263.

(22) Orlova, A.; Egelman, E. H. Structural Dynamics of F-actin I. Changes in the C Terminus. *J. Mol. Biol.* **1995**, *245*, 582−597.

(23) Fan, J.; Saunders, M. G.; Voth, G. A. Coarse-Graining Provides Insights on the Essential Nature of Heterogeneity in Actin Filaments. *Biophys. J.* **2012**, *103*, 1334−1342.

(24) Saunders, M. G.; Voth, G. A. Comparison Between Actin Filament Models: Coarse-Graining Reveals Essential Differences. *Structure* **2012**, *20*, 641−653.

(25) Fujii, T.; Iwane, A. H.; Yanagida, T.; Namba, K. Direct Visualization Of Secondary Structures Of F-Actin By Electron Cryomicroscopy. *Nature* **2010**, *467*, 724−728.

(26) Oda, T.; Iwasa, M.; Aihara, T.; Maeda, Y.; Narita, A. The Nature of the Globular- to Fibrous-actin Transition. *Nature* **2009**, *457*, 441−445.

(27) Otterbein, L. R.; Graceffa, P.; Dominguez, R. The Crystal Structure of Uncomplexed Actin in the ADP State. *Science* **2001**, *293*, 708−711.

(28) Mackerell, A. D.; Feig, M.; Brooks, C. L. Extending the Treatment of Backbone Energetics in Protein Force Fields: Limitations of Gas-Phase Quantum Mechanics in Reproducing Protein Conformational Distributions in Molecular Dynamics Simulations. *J. Comput. Chem.* **2004**, *25*, 1400−1415.

(29) Jorgensen, W. L.; Chandrasekhar, J.; Madura, J. D.; Impey, R. W.; Klein, M. L. Comparison of Simple Potential Functions for Simulating Liquid Water. *J. Chem. Phys.* **1983**, *79*, 926−935.

(30) Phillips, J. C.; Braun, R.; Wang, W.; Gumbart, J.; Tajkhorshid, E.; Villa, E.; Chipot, C.; Skeel, R. D.; Kalé, L.; Schulten, K. Scalable Molecular Dynamics with NAMD. *J. Comput. Chem.* **2005**, *26*, 1781−1802.

(31) Humphrey, W.; Dalke, A.; Schulten, K. VMD: Visual Molecular Dynamics. *J. Mol. Graphics* **1996**, *14*, 33−38.

(32) Darden, T.; York, D.; Pedersen, L. Particle Mesh Ewald: An N•log(N) Method for Ewald Sums in Large Systems. *J. Chem. Phys.* **1993**, *98*, 10089−10092.

(33) Feller, S. E.; Zhang, Y.; Pastor, R. W.; Brooks, B. R. Constant Pressure Molecular Dynamics Simulation: The Langevin Piston Method. *J. Chem. Phys.* **1995**, *103*, 4613−4621.

(34) Steinhardt, P. J.; Nelson, D. R.; Ronchetti, M. Bond-Orientational Order in Liquids and Glasses. *Phys. Rev. B: Condens. Matter Mater. Phys.* **1983**, *28*, 784−805.

(35) Altis, A.; Nguyen, P. H.; Hegger, R.; Stock, G. Dihedral Angle Principal Component Analysis of Molecular Dynamics Simulations. *J. Chem. Phys.* **2007**, *126*, 244111.

(36) Coifman, R. R.; Lafon, S.; Lee, A. B.; Maggioni, M.; Nadler, B.; Warner, F.; Zucker, S. W. Geometric Diffusions as a Tool for Harmonic Analysis and Structure Definition of Data: Diffusion Maps. *Proc. Natl. Acad. Sci. U. S. A.* **2005**, *102*, 7426−7431.

(37) Ferguson, A. L.; Panagiotopoulos, A. Z.; Kevrekidis, I. G.; Debenedetti, P. G. Nonlinear Dimensionality Reduction in Molecular Simulation: The Diffusion Map Approach. *Chem. Phys. Lett.* **2011**, *509*, 1−11.

(38) Theobald, D. L. Rapid Calculation of RMSDs Using a Quaternion-Based Characteristic Polynomial. *Acta Crystallogr., Sect. A: Found. Crystallogr.* **2005**, *61*, 478−480.

(39) McGibbon, R. T.; Beauchamp, K. A.; Harrigan, M. P.; Klein, C.; Swails, J. M.; Hernández, C. X.; Schwantes, C. R.; Wang, L.-P.; Lane, T. J.; Pande, V. S. MDTraj: A Modern Open Library for the Analysis of Molecular Dynamics Trajectories. *Biophys. J.* **2015**, *109*, 1528−1532.

(40) Baker, J. L.; Voth, G. A. Effects of ATP and Actin-Filament Binding on the Dynamics of fhe Myosin II S1 Domain. *Biophys. J.* **2013**, *105*, 1624−1634.

(41) Holmes, K. C.; Popp, D.; Gebhard, W.; Kabsch, W. Atomic Model of the Actin Filament. *Nature* **1990**, *347*, 44−49.

(42) Galkin, V. E.; Orlova, A.; Vos, M. R.; Schröder, G. F.; Egelman, E. H. Near-Atomic Resolution for One State of F-Actin. *Structure* **2015**, *23*, 173−182.

(43) Galkin, V. E.; Orlova, A.; Egelman, E. H. Actin Filaments as Tension Sensors. *Curr. Biol.* **2012**, *22*, R96−R101.

(44) Berman, H. M.; Westbrook, J.; Feng, Z.; Gilliland, G.; Bhat, T. N.; Weissig, H.; Shindyalov, I. N.; Bourne, P. E. The Protein Data Bank. *Nucleic Acids Res.* **2000**, *28*, 235−242.

(45) von der Ecken, J.; Muller, M.; Lehman, W.; Manstein, D. J.; Penczek, P. A.; Raunser, S. Structure of the F-actin-Tropomyosin Complex. *Nature* **2015**, *519*, 114−117.

(46) Furuhashi, K.; Hatano, S.; Ando, S.; Nishizawa, K.; Inagaki, M. Phosphorylation by Actin Kinase of the Pointed End Domain on the Actin Molecule. *J. Biol. Chem.* **1992**, *267*, 9326−9330.

(47) Sonobe, S.; Takahashi, S.; Hatano, S.; Kuroda, K. Phosphorylation of Amoeba G-actin and its Effect on Actin Polymerization. *J. Biol. Chem.* **1986**, *261*, 14837−14843.

(48) Cao, W.; Goodarzi, J. P.; De La Cruz, E. M. Energetics and Kinetics of Cooperative Cofilin−Actin Filament Interactions. *J. Mol. Biol.* **2006**, *361*, 257−267.

(49) Hung, R.-J.; Pak, C. W.; Terman, J. R. Direct Redox Regulation of F-Actin Assembly and Disassembly by Mical. *Science* **2011**, *334*, 1710−1713.

(50) Frishman, D.; Argos, P. Knowledge-Based Protein Secondary Structure Assignment. *Proteins: Struct., Funct., Genet.* **1995**, *23*, 566−579.

(51) De La Cruz, E. M.; Roland, J.; McCullough, B. R.; Blanchoin, L.; Martiel, J.-L. Origin of Twist-Bend Coupling in Actin Filaments. *Biophys. J.* **2010**, *99*, 1852−1860.

(52) Prochniewicz, E.; Janson, N.; Thomas, D. D.; De La Cruz, E. M. Cofilin Increases the Torsional Flexibility and dynamics of Actin Filaments. *J. Mol. Biol.* **2005**, *353*, 990−1000.

(53) Galkin, V. E.; Orlova, A.; Schroder, G. F.; Egelman, E. H. Structural Polymorphism in F-Actin. *Nat. Struct. Mol. Biol.* **2010**, *17*, 1318−1323.

(54) Dama, J. F.; Sinitskiy, A. V.; McCullagh, M.; Weare, J.; Roux, B.; Dinner, A. R.; Voth, G. A. The Theory of Ultra-Coarse-Graining. 1. General Principles. *J. Chem. Theory Comput.* **2013**, *9*, 2466−2480.

(55) Davtyan, A.; Dama, J. F.; Sinitskiy, A. V.; Voth, G. A. The Theory of Ultra-Coarse-Graining. 2. Numerical Implementation. *J. Chem. Theory Comput.* **2014**, *10*, 5265−5275.